Regulation of Cell Cytoskeleton and Membrane Mechanics by Electric Field: Role of Linker Proteins

Igor Titushkin and Michael Cho*
Department of Bioengineering, University of Illinois, Chicago, Illinois 60607

ABSTRACT Cellular mechanics is known to play an important role in the cell homeostasis including proliferation, motility, and differentiation. Significant variation in the mechanical properties between different cell types suggests that control of the cell metabolism is feasible through manipulation of the cell mechanical parameters using external physical stimuli. We investigated the electrocoupling mechanisms of cellular biomechanics modulation by an electrical stimulation in two mechanically distinct cell types—human mesenchymal stem cells and osteoblasts. Application of a 2 V/cm direct current electric field resulted in approximately a twofold decrease in the cell elasticity and depleted intracellular ATP. Reduction in the ATP level led to inhibition of the linker proteins that are known to physically couple the cell membrane and cytoskeleton. The membrane separation from the cytoskeleton was confirmed by up to a twofold increase in the membrane tether length that was extracted from the cell membrane after an electrical stimulation. In comparison to human mesenchymal stem cells, the membrane-cytoskeleton attachment in osteoblasts was much stronger but, in response to the same electrical stimulation, the membrane detachment from the cytoskeleton was found to be more pronounced. The observed effects mediated by an electric field are cell type- and serum-dependent and can potentially be used for electrically assisted cell manipulation. An in-depth understanding and control of the mechanisms to regulate cell mechanics by external physical stimulus (e.g., electric field) may have great implications for stem cell-based tissue engineering and regenerative medicine.

INTRODUCTION

Various biological systems have been reported to respond to endogenous and exogenous electromagnetic fields (1–3). Many living tissues exhibit naturally occurring electrical activities. Examples include transepithelial potentials (~mV range) in glands and embryos (4), specific transendothelial extracellular potential gradients in blood vessels (5), electrical fields of strengths as large as 2 V/cm detected at wound sites (6). These observations suggest that physiologically relevant electric fields can be used as an efficient tool to control cellular and tissue homeostasis. Indeed, external electric field has been shown to induce a variety of cellular and molecular responses including microfilament reorganization (7,8), cell surface receptor redistribution (9,10), changes in intracellular calcium dynamics (11–13), galvanotropic cell migration and orientation (14,15), neuronal growth cone guidance (16), enhanced stem cell differentiation (17,18), and angiogenesis (19,20). Moreover, electrotherapy has been successfully used clinically for bone fracture treatment, nerve fiber repair, soft tissue regeneration, and cancer chemotherapy (21–25). Several modes of electrical stimulation have been tried in various in vitro and in vivo experiments, including direct current (dc), pulsed, alternating current electric field, and magnetically induced electrical stimulation (26,27). For consistent success in the interpretation of clinical studies, careful assessment of electrical stimulation characteristics such as strength, frequency, and exposure duration would be required. However, selection of these electrical parameters remains mainly empirical, because biochemical and biophysical electrocoupling mechanisms mediating cellular responses to electrical stimulation remain not fully identified. For example, a very little information is available about the effect of electric field on the cell mechanical properties. Yet, cell biomechanics has been shown to play a crucial role in many vital cellular processes including proliferation, adhesion, motility, and differentiation (28).

Cell adapts to its biomechanical environment by adjusting its mechanical properties to match those of the surrounding tissue. Cytoskeleton is one of the most significant cellular mechanical components and provides structural stability and elasticity to the cell undergoing multiple deformations without losing its integrity (29,30). In addition, an important role of the cytoskeleton in complex intracellular signaling pathways has now been established (31). Its function as a mechanotransducer is attributed to the cytoskeleton-associated members of numerous signaling cascades, such as Rho family GTPases (32). In this way, the cytoskeleton mediates cell response to changing biomechanical environment (e.g., substrate stiffness, cell shape and deformation, external pressure, shear stress) by structural rearrangement of the cytoskeleton itself, or alterations in gene expression profiles, cell adhesion, and secretion of extracellular matrix (29,33).

Another important mechanical element of the cell is its plasma membrane. Beside its function as a barrier from the outer environment, it participates in inward-outward trafficking, motility, and cell-cell interaction (34,35). These and many other intracellular events are regulated by the membrane surface tension, which is maintained by multiple

Submitted March 5, 2008, and accepted for publication September 30, 2008.
*Correspondence: mcho@uic.edu
Editor: Marileen Dogterom.

0006-3495/09/01/0717/12 $2.00
doi: 10.1016/j.bpj.2008.09.035

mechanisms including membrane reservoir and lipid material turnover (35,36). Generally, the membrane tension is determined by the lipid bilayer composition such as cholesterol content (37), and the membrane interaction with the cytoskeleton via specific biomolecular linkage systems (38). We have shown recently that the plasma membrane attachment to the cytoskeleton in fully differentiated osteoblasts is much stronger than in undifferentiated stem cells (39). Functionally, a strong membrane-cytoskeleton adhesion should be beneficial to keep the structural integrity of osteoblasts subjected to continuous stress cycles. On the other hand, in human mesenchymal stem cells (hMSCs) a lower membrane tension may better facilitate endo- and exocytosis and contributes to a higher sensitivity of these cells to various soluble biochemical environmental stimuli.

The cells of mesodermal origin show a wide spectrum of mechanical properties. This observation opens an exciting perspective to regulate cell homeostasis by controlling its biomechanics. Indeed, specific types of mechanical stimulation (e.g., shear stress, cyclic stretching, compressive loading) can be used for regulation of gene expression, matrix components secretion, cell differentiation, and ultimately engineering functional load-bearing tissues (29,40). We have shown previously that mesenchymal stem cells are mechanically strikingly different from fully differentiated osteoblasts, and the mechanical properties are altered during osteodifferentiation (41). This finding suggests that control of cell differentiation is feasible through manipulation of the cell mechanical properties using external physical stimuli. Therefore, systematic investigations of the cell mechanics modulation by external physical stimulus (e.g., electric field) would allow targeted regulation of cell metabolism through control of cell biomechanics (27). This information will have great implications for tissue engineering and regenerative medicine. For example, elucidation of the electrocoupling mechanisms is expected to establish a rationale paradigm for electrically assisted differentiation of stem cells into preselected phenotypic lineage. In this study, we examined the effect of dc electric fields on the mechanical properties of two model cell types: hMSCs and fully differentiated human osteoblasts. We investigated the molecular mechanisms of electrically induced mechanical changes in the cell membrane and cytoskeleton. Careful characterization of electrically stimulated and cell type-dependent mechanical responses could lead to enhance cell differentiation (18) and other tissue engineering applications.

MATERIALS AND METHODS

Cell culture and drug treatment

Human mesenchymal stem cells were obtained from the Tulane Center for Gene Therapy (New Orleans, LA). Based on flow cytometry results, these stem cells showed negative staining for CD34, CD36, CD45, and CD117 markers (all <2%), and positive staining for CD44, CD90, CD166, CD29, CD49c, CD105, and CD147 markers (all >95%), indicating a minimal heterogeneity in cell population. Normal human fetal osteoblasts (hFOB 1.19) were obtained from American Tissue Culture Collection (Manassas, VA). Cells were grown in Dulbecco's modified Eagle's culture medium with 15% fetal bovine serum, L-glutamin, and antibiotics. Two days before experiments, cells were harvested and plated on a 24 × 30 mm glass coverslip. Cells were rinsed gently with Hanks' balanced salt solution (HBSS) and mounted on the electrical stimulation exposure chamber, AFM fluid chamber, or sealed coverglass chamber for optical trapping. Cells between passages 3 and 12 were used for all experiments.

For ATP depletion, cells were incubated in PBS containing the mitochondria inhibitor sodium azide (10 mM) and glycolytic inhibitor 2-deoxyglucose (10 mM) for 40–60 min at 37°C. Ionomycin (10 μM) was used to equilibrate intracellular and extracellular calcium levels. All drugs were purchased from Sigma-Aldrich (St. Louis, MO).

Electric field exposure

The chamber used to stimulate cell with an electric field has been described earlier (9,11,14). Joule heating was minimized by incorporating a sapphire window and a large surface/volume ratio in the chamber design. Agarose salt bridges were used in the experiments to eliminate unwanted electrode byproducts and to minimize pH changes. Electrical current was supplied to the chamber by a 100 W amplifier (BOP100, Kepco, Flushing, NY) and monitored by an oscilloscope (Tektronix, Model 2205, Beaverton, OR). The computation of electric field strength E followed Ohm's law, $J = \sigma E$, where J is the electric current density and σ is the conductivity of the medium. Electric field application was carried out in HBSS or cell culture medium at room temperature. Temperature rise caused by application of a 2 V/cm field for 60 min was negligible (12).

AFM microindentation test

The live cell elasticity was measured with a Novascan atomic force microscope (Novascan Technologies, Ames, IA) mounted on an inverted TE-2000 Nikon microscope. Soft silicone nitride cantilevers (100 μm long, Veeco, Santa Barbara, CA) were calibrated by the thermal fluctuation method in air (42), with a typical spring constant value of 0.12 N/m. Borosilicate glass beads (10 μm in diameter) glued onto the cantilever served as spherical cell indenters. Distribution of the indenting load over several-micron area allows to remove spatial mechanical heterogeneity of fibrous cell cytoskeleton. Individual isolated cells with normal morphology were mechanically probed with AFM, avoiding the cell's perinuclear region. To obtain a force curve, the cantilever descended toward the cell at a velocity of ~2 μm/s until a trigger force of 3 nN was reached, and then retracted. Viscous dissipation of energy is minimal at this speed, and force measurements are dominated by the elastic behavior of the cell (41). To minimize the effect of glass substrate on the cell elasticity measurements, we used an indentation depth up to 500 nm (~10–15% of the average cell height) for data analysis. A total of 30–40 cells of each type and experimental condition were used, with ~15 force-distance curves acquired from each cell. The force-distance curves were collected and analyzed according to the Hertz model (43,44), which relates the loading force (F) with the indentation depth (δ) by

$$F = \frac{4}{3}\frac{E}{(1-\nu^2)}\delta^{3/2}\sqrt{R},$$

where ν is the cellular Poisson's ratio, R is the radius of the spherical indenter (5 μm), E is the local Young's elastic modulus. The cellular Poisson's ratio was assumed to be 0.5, which treats the cell as an incompressible material (44). Fitting the Hertz model to the experimental force curve with a standard least squares minimization algorithm yielded the local apparent elastic modulus E. The average Young's modulus for each cell type and experimental condition was calculated and subjected to t-test at the level of 0.05.

Membrane tether extraction with laser optical tweezers

Fluorescent polystyrene beads 0.5 μm diameter with 515-nm emission (FluoSpheres, Molecular Probes, Eugene, OR) were covalently coated with mouse anti-CD29 antibodies and tightly bound to the cell membrane. The beads were used as handles for a membrane tether extraction, as described earlier (39,45). An infrared Nd:YAG laser (1064 nm, continuous wave, 0.5 W maximum incident power at the sample; SpectraPhysics, Mountain View, CA) with a Nikon Eclipse E-800 microscope was used for particle optical trapping. The laser beam was focused at the cell surface with a 100× oil immersion microscope objective (PlanApo, NA 1.4), and this optical trap was moved in the focus plane by a system of two confocal lenses actuated by a high-precision motorized translator. Cells, laser, and fluorescent beads were imaged with a 16-bit charge-coupled device camera (Photometrics, Tucson, AZ) in the bright-field and epifluorescence modes. To extract a membrane tether from the cell, a latex bead attached to the cell was chosen randomly and optically trapped. The bead was then displaced from its equilibrium position by moving the trap away from the cell at a constant speed of 1.5 μm/s and a constant force ~3 pN. The Stoke's drag in an aqueous solution and the membrane viscosity have negligible effects on the bead dynamics at this speed. Tether growth was observed until the bead escaped from the trap. Elastic membrane tether formation was identified by quick retraction of the bead to its original position after escape from the trap. The total tether length was determined by tracking bead position using the MetaMorph image processor (Molecular Devices, Downingtown, PA). Typically, 35–40 beads from ~20 cells were analyzed for each experimental condition and cell type. Differences in tether length were examined using Student's *t*-test. Results were deemed statistically significant when $p < 0.05$.

Immunostaining and fluorescence microscopy

To explore the cytoskeleton structure and linker protein distribution of normal and electrically stimulated cells, the samples were fixed in 3.7% formaldehyde and permeabilized in cold (−20°C) acetone for 3 min. Nonspecific binding sites were blocked using a 1% bovine serum albumin solution for 30 min at room temperature. Intracellular actin filaments were stained with rhodamine-phalloidin (5 μM) for 30 min at room temperature (Molecular Probes). Ezrin/radixin/moesin (ERM) proteins were labeled with rabbit ERM antibody (Cell Signaling Technology, Danvers, MA), and secondary goat anti-rabbit antibody conjugated with AlexaFluor488 dye (Molecular Probes). Focal adhesions were labeled using mouse antibody to vinculin (Chemicon, Temecula, CA), and secondary fluorescent goat anti-mouse antibody.

Samples were imaged by a laser scanning confocal system (Radiance 2001MP, Bio-Rad, Hercules, CA) operating on a Nikon TE2000-S inverted microscope with a 60× Plan Apo objective (NA 1.4), blue Argon ion (488 nm), and green HeNe (543 nm) lasers. Emission filters (515/30 nm and 600/50 nm) were used to collect confocal images of ERM and microfilaments, respectively.

Relative F-actin concentration was determined by fluorescent microscopy as described elsewhere (8,46). In brief, after fixation and permeabilization the cells were stained with rhodamine-phalloidin (5 μM) to visualize actin and AlexaFluor488 succinimidyl ester dye (10 μM) to label total cell protein. The rhodamine-phalloidin and succinimidyl ester images of the same region were obtained using an E-800 Eclipse Nikon fluorescent microscope with a 20× objective lens and a 16-bit charge-coupled device camera (Photometrics). The edges of the cells on a total protein image were used to define the mask for these cells. After background subtraction, F-actin and total protein contents were measured by summing the total fluorescence intensity signal on the masked images of corresponding fluorophores. The relative F-actin content was then obtained by dividing F-actin by total protein for each cell, and normalizing it to the corresponding control sample. Different experimental groups of cells were stained using the same solutions and imaged identically with their respective controls.

Total protein images of the cells were also used for morphological analysis including cell surface area and form factor measurements. The form factor F was calculated as $F = 4\pi A/P^2$, where A is a cell surface area, and P is its perimeter. Smaller F values indicate more complex cell geometry, and higher deviation of cell shape from an ideal circle ($F = 1$).

Bioluminescent ATP measurements

Intracellular ATP content was determined using a luciferin-luciferase assay (Sigma, St. Louis, MO) in a SPECTRAmax Gemini XS Microplate Spectrofluorometer (Molecular Devices, Sunnyvale, CA). A glass coverslip with normal or electrically exposed cells was washed with PBS and treated with 300 μl of somatic cell ATP releasing agent. The sample was collected into a vial and mixed with an equal volume of diluted ATP assay mix, and amount of emitted light was measured immediately with a luminometer. In control experiments the background chemiluminescence signal from cell buffer was determined. In each series of experiments, ATP content was normalized to the values from respective control samples.

Gel electrophoresis and Western blotting

The expression levels of ERM proteins were analyzed using immunoblotting. Equal amounts of protein per well were diluted in Laemmli sample buffer (BioRad, Hercules, CA), boiled for 3 min, subjected to 8% SDS-PAGE, and transferred to PVDF membrane. The membranes were washed with Tris-buffered saline + Tween (TBST, 0.01 M Tris · HCl Ph 7.4, 0.15 NaCl, and 0.1% Tween 20), blocked with 5% nonfat dry milk solution in TBST, incubated with appropriate primary antibody, and horseradish peroxidase-conjugated secondary antibody. Antibody recognizing total ERM, and ezrin, radixin, and moesin phosphorylated at Thr^{567}, Thr^{564}, Thr^{558}, respectively (corresponding to the active state of these proteins) were purchased from Cell Signaling (Beverly, MA). Antibody binding was visualized with Opti-4CN detection kit (BioRad). Membranes were scanned using GelDoc XR system (BioRad), and the band densiometric measurements were carried out with BioRad Quantity One software. The total level of ERM, i.e., the sum of the ~80 kDa band (corresponding to ezrin and radixin) and the ~75 kDa band (corresponding to moesin) was obtained. The phospho-ERM level was normalized to the corresponding total ERM level in each sample, and taken relative to the untreated cell value.

RESULTS

Cell cytoskeleton elasticity measurement

To investigate changes in the cell elastic properties induced by an electrical stimulation, we used AFM indentation technique as described earlier (41). As shown previously, the average elastic modulus of normal hMSCs (3.2 ± 1.4 kPa) is almost a twofold higher than that of fully differentiated osteoblasts (1.7 ± 1.0 kPa; Fig. 1 *A*). Exposure of cells to a 2 V/cm electric field for 60 min in HBSS resulted in a decrease in the cell elasticity to 1.0 ± 0.5 kPa in hMSCs and to 1.1 ± 0.5 kPa in osteoblasts (Fig. 1 *A*). Similar results were observed after cell treatment with calcium ionophore, which causes an influx of calcium ions into the cytoplasm from extracellular medium. Increases in intracellular calcium concentration in response to electrical stimulation have been reported by multiple laboratories (2,11,12,47), and were also detected in our experiments using the fluorescent calcium indicator Fluo-4 (data not shown). We should note that the cell type-dependent dynamics of elastic changes is rather remarkable. For example, within 60 min of an electrical

stimulation, the hMSC elasticity decreased ~70% whereas osteoblasts showed only a ~30% elasticity reduction under the similar experimental conditions. Measurements of the cell elastic moduli at intermediate time points (e.g., 30, 45 min dc field exposure) support the data on a faster elasticity decrease in the hMSC cytoskeleton in comparison with osteoblasts. Interestingly, when the cells were electrically stimulated in complete growth medium, only a minimal decrease in cell stiffness was observed (Fig. 1 *A*). For example, an electrical stimulation in culture medium caused higher data dispersion and only a statistically insignificant decrease in the osteoblast cytoskeleton elasticity. Decrease in the elastic modulus can be partially reversed up to 60–80% of the original value by incubating the cells in culture medium for 60 min (data not shown), implying an important role of serum in mediating electric field effect on the cellular mechanics.

As reported earlier, actin is the major determinant of the cytoskeleton elasticity rather than microtubules or intermediate filaments (41,48). We therefore measured relative F-actin content in the cells after an electric stimulation. In both cell types the amount of polymerized actin decreased after electric field exposure or ionomycin treatment in HBSS (Fig. 1 *B*). Consistent with our observation, this decrease is less pronounced when the cells were exposed to the electric field in the culture medium with serum. In addition, cell viability assays showed that no less than 90% cells were viable after 60 min of electrical field stimulation and/or AFM mechanical testing. A longer exposure of cells to the electric field up to 90 min produces only a minor further decrease in the cell elasticity, but adversely affects cell viability. Variation of dc electric field strength in the range 0.5–3 V/cm produced similar commensurate effects in the cell elastic properties, which is qualitatively similar to those reported here using a 2 V/cm field.

Electrically induced actin reorganization

Significant differences in the cellular mechanics between hMSCs and osteoblasts are likely to result from differential actin organization in these cells. For example, actins in osteoblasts are predominantly organized as thin dense filamentous meshwork with focal contacts that are generally round and smaller in size (Fig. 2 *A*). In contrast, stem cells show many thick actin bundles, or stress fibers, extending throughout the cytoplasm and terminating at focal contacts (41) that are irregularly shaped and much larger in size (Fig. 2 *B*), possibly indicative of a stronger adhesion to the substrate, as indicated by vinculin labeling. After an electrical stimulation of cells in HBSS, both actin structures were impaired (Fig. 2, *C* and *D*). Disassembly of actin scaffolds

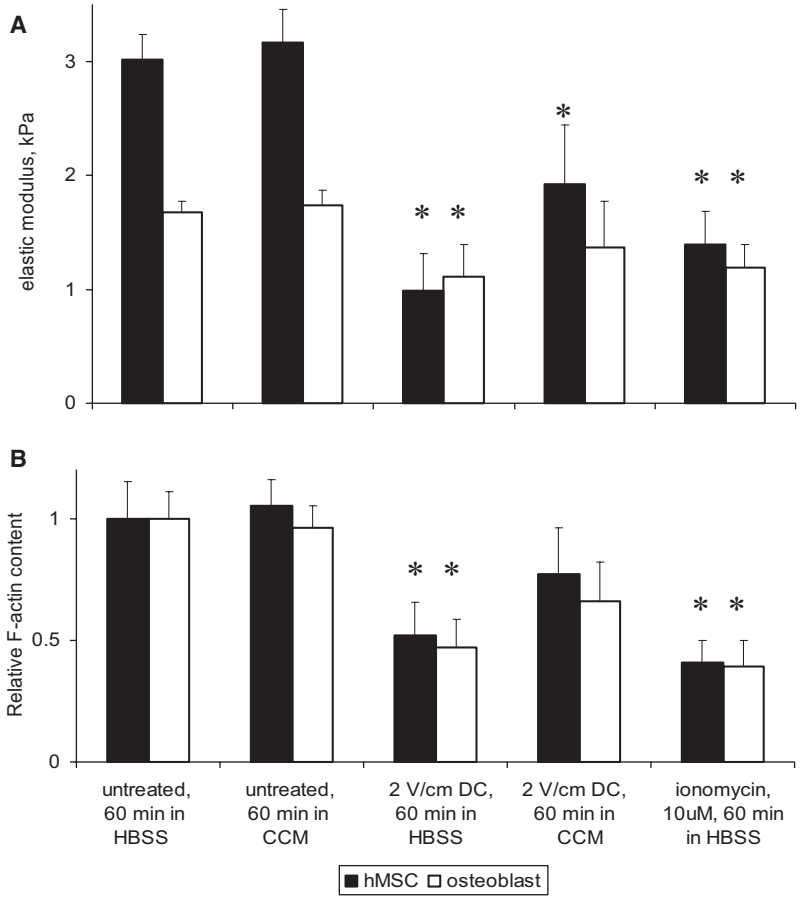

FIGURE 1 Effect of electric field on cell cytoskeleton. Cells were exposed to a 2 V/cm dc field for 60 min in HBSS, and complete cell culture medium (CCM). (*A*) Cell cytoskeleton elasticity determined with AFM microindentation. The elastic modulus decreased significantly after an electrical stimulation or cell treatment with calcium ionophore in HBSS in both hMSCs and osteoblasts. Between 400–600 force-curves were acquired for each cell type and experimental condition. (*B*) Relative F-actin content in cells exposed to the electric field. It was obtained for each cell as a ratio of fluorescence signals from F-actin and the total protein, and then normalized to the corresponding control. The highest degree of actin depolymerization was observed in electrically stimulated cells in the absence of serum. Results represent the mean ± SE. *Statistically different from respective controls ($p < 0.05$).

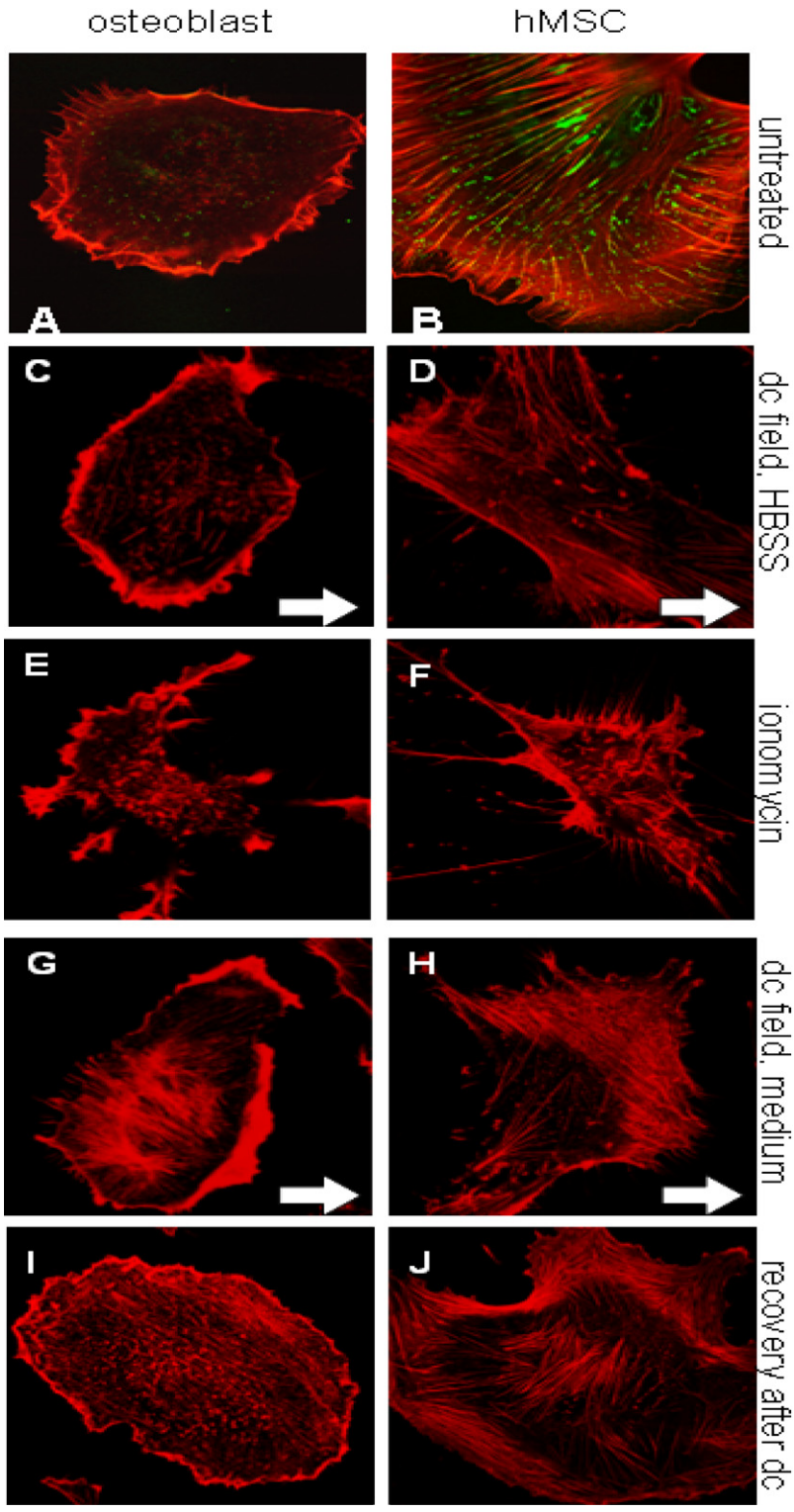

FIGURE 2 Actin cytoskeleton reorganization. Fluorescent images of osteoblasts are in the left column and hMSCs in the right column. Immunofluorescent images of a thin filamentous actin meshwork (*red*) and vinculins (*green*) showed that osteoblasts contain fewer and smaller focal adhesions (*A*). In contrast, hMSCs showed thick actin stress fibers, and multiple and large adhesion contacts (*B*). Actins were partially disassembled in both osteoblast (*C*) and hMSC (*D*) after cell exposure to a 2 V/cm field for 60 min in serum-free HBSS. Cells treatment with 10 μM ionomycin for 40 min in HBSS produced analogous actin dismantling effects both in osteoblast (*E*) and hMSC (*F*). When cells were placed in cell culture medium with serum, the electrical stimulation again caused redistribution of actins in osteoblast (*G*) and stem cells (*H*), but in a manner that was different than (*C*) and (*D*) without serum. Cell incubation in the complete culture medium for 60 min at 37°C after the dc field exposure resulted in a partial recovery of the actin structure in both osteoblasts (*I*) and hMSC (*J*). The arrows indicate the direction of the electric field applied.

seems to be responsible for decrease in the cellular elasticity. Interestingly, we did not observe electrically induced changes in microtubule or intermediate filament arrangement. Cell treatment with ionomycin, however, caused similar breakdown of actin cytoskeleton as did an electric field (Fig. 2, *E* and *F*). The actin cytoskeleton reorganization was noticeably different and appeared more complex when cells placed in the complete culture medium with serum were exposed to an electric field (Fig. 2, *G* and *H*). Actins were clearly accumulated toward the cathode side and actin depolymerization was noticeably visible at the anode side of the cell. This anisotropic actin redistribution is typical for

serum-dependent cell galvanotaxis that has been reported elsewhere (10,15). Indeed, we observed some electromigration of osteoblasts, but not hMSCs, toward the cathode (data not shown). This is likely due to stronger substrate adhesion of hMSC compared to osteoblasts as implied by abundance and larger size focal contacts terminating multiple stress fibers in stem cells (see Fig. 2 *B*). This cell type-dependent differential cell adhesion is consistent with our previous report that the integrins on the surface of undifferentiated hMSCs were found to be clustered and laterally immobile (i.e., confined or restricted) until hMSCs undergo osteodifferentiation (49). Finally, the electrically mediated actin remodeling was reversible as shown by incubating the cells in the complete culture medium for 60 min after an electric field exposure (Fig. 2, *I* and *J*). The actin cytoskeleton arrangement seems to have been restored to its original structure in both cell types. As mentioned earlier, this actin structural repair was accompanied by a recovery of the cell stiffness almost to its original values.

Membrane mechanical properties

Fluorescent polystyrene beads attached to the cell plasma membrane were pulled with a laser optical trap to produce thin lipid membrane tethers. Binding specificity of antibody-coated probes has been verified in control experiments with noncoated beads; ~20–40% of membrane-conjugated beads were fluctuating on the cell surface and could be used for tether extraction. Short exposure to the laser (~15–30 s to pull one tether) allows to avoid laser-induced photo damage as confirmed by repeating experiments using the same bead with consistently reproducible results. The average tether length in normal hMSC (10.6 ± 1.1 μm) is ~2.5-fold higher than that in osteoblasts (4.0 ± 1.1 μm) (Fig. 3 *A*). As we postulated earlier, this result is due to much weaker membrane-cytoskeleton interaction in stem cells compared to osteoblasts (39). Cell exposure to a 2 V/cm electric field resulted in a twofold tether length increase in osteoblast, but had no significant effect on the tether length in stem cells (Fig. 3 *A*). Similar results were achieved by intracellular ATP depletion with sodium azide and 2-deoxyglucose. To test if the electric field effect on the membrane tether length is mediated by ATP, we measured the ATP content in the cell before and after an electrical stimulation. As expected, the intracellular ATP level decreased in response to an electric field (Fig. 3 *B*). This result is consistent with earlier findings suggesting ATP release from the cells in response to electrical stimulation (47,50). Unfortunately, we could not detect measurable traces of released ATP in the electrical exposure chamber due to a high volume of buffer/medium filling the chamber. However, unlike osteoblasts, we could not find statistically significant changes in the tether length in stem cells in response to the electric field or ATP depletion. Apparently, the current optical trapping technique sensitivity is not sufficient to detect further minor electrically induced decrease in the originally weak hMSC membrane-cytoskeleton adhesion.

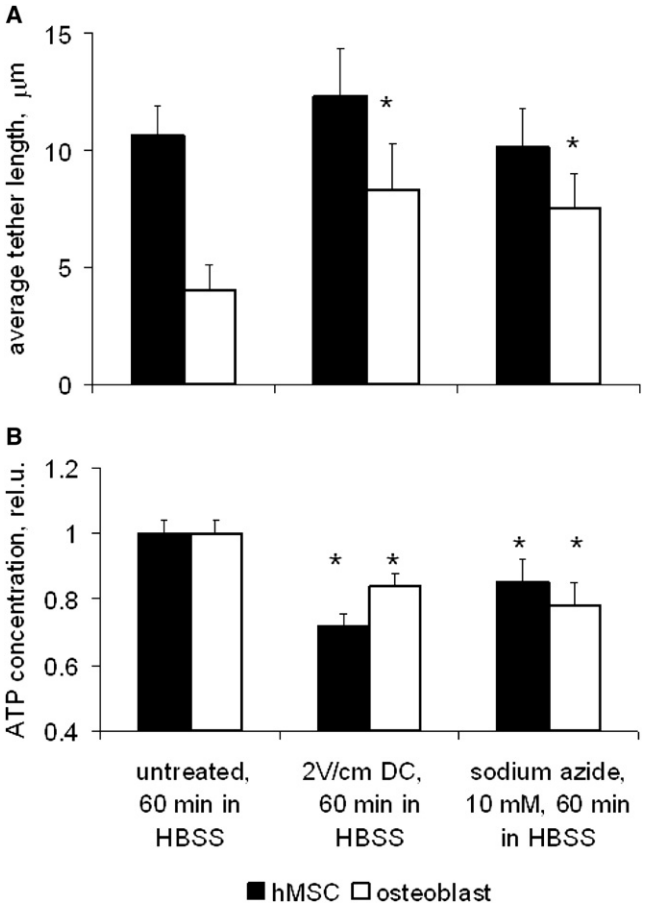

FIGURE 3 Electrically induced changes in the plasma membrane mechanics. (*A*) Membrane tether length measured with laser optical tweezers. Much longer tethers could be extracted from the normal hMSC membrane than that of osteoblasts, likely due to a weaker membrane-cytoskeleton interaction in stem cells. The tether lengths increased in osteoblasts after cell exposure to a 2 V/cm field or 10 mM sodium azide and 10 mM 2-deoxyglucose. At least 30 tethers were measured for each cell type and experimental condition. (*B*) Intracellular ATP content determined with bioluminescent luciferin-luciferase assay. The ATP content was normalized to untreated samples. Results represent the mean ± SE. *Statistically different from respective controls ($p < 0.05$).

ERM linker protein response to electrical stimulation

The membrane-cytoskeleton interaction is mediated by special linker proteins that physically couple the membrane with the cytoskeleton. For instance, the ERM family proteins are found in the cytoplasm of many cell types. On activation these proteins can bind both to polymerized actin and integral membrane proteins (51–53). For example, a dense actin network underlying the osteoblasts plasma membrane provides high density binding sites for the ERM proteins that are distributed uniformly (Fig. 4 *A*). In contrast, in hMSCs there are relatively few binding sites for the ERM linkers on the sparse actin stress fibers proximal to the plasma membrane, and the ERM proteins were found

to be located primarily along stress fibers underlying the membrane (Fig. 4 *D*). In response to an electrical stimulation (Fig. 4, *B* and *E*) or ATP depletion (Fig. 4, *C* and *F*), the amount of these linker proteins seemed to have decreased. Moreover, there is a clear correlation between inhibition of the ERM proteins and the membrane-cytoskeleton separation in osteoblasts. The ERM protein redistribution in hMSCs in response to an electrical stimulation or ATP depletion is much less pronounced than in osteoblasts, and the corresponding changes in the membrane tether length were not significant statistically.

Immunoblotting of the total and phosphorylated ERM proteins in osteoblasts and hMSCs confirmed that the relative amount of activated linker proteins decreased after cell exposure to a dc electric field or metabolic inhibitors such as sodium azide and 2-deoxyglucose (Fig. 5). For example, after an electrical stimulation or sodium azide treatment, both cell types showed a ~1.5–2-fold decrease in the immunoblot-detected signal corresponding to phosphorylated (i.e., activated) ERM linkers as compared to that measured in untreated cells. Although an accurate quantitative phospho-ERM concentration decrease can not be directly inferred from immunoblotting results, this finding does suggest a significant inhibition of the ERM proteins by an electric field.

Altered cellular morphology

Cellular morphological properties are closely related to the cell mechanics. For example, a stronger adhesion to the glass substrate of hMSCs than osteoblasts is attributed to multiple focal contacts and stress fibers in stem cells (see Fig. 2 *B*). As result, hMSCs have a much higher surface area on 2D substrate than osteoblasts (Table 1), and a more stretched and edgy cell morphology was observed as indicated by a lower form-factor compared to osteoblasts. Stimulation with a 2 V/cm electric field for 40 min seemed to decrease both the surface area and the form-factor in the two cell types (i.e., smaller size cells and more complex spiky geometry). Apparently, electrically induced morphological changes are due to both actin cytoskeleton reorganization and membrane-cytoskeleton dissociation. Indeed, ionomycin-mediated actin depolymerization caused a significant decrease in the cell area and the form factor in both cell types. Besides, loosening the tight membrane-cytoskeleton attachment in osteoblasts by ATP depletion also led to a decrease in the form factor in these cells (Table 1). Severe changes in the cell morphology may result in activation of stretch-activated cation channels causing additional Ca^{2+} influx and further actin reorganization.

DISCUSSION

Multiple biochemical and biophysical responses to exogenous electric field have serious implications to the cell metabolism. This study shows that the cellular biomechanics can be modulated considerably by an externally applied electric field. The cell elasticity decreases due to substantial actin cytoskeleton reorganization during exposure to an external dc electric field. Direct current and low frequency alternating current electric fields are unable to penetrate into the cell interior due to high resistivity of the cell membrane (membrane conductivity is ~10^6–10^8 times smaller than that of the cytoplasm (54), excluding direct coupling to actins. Therefore, molecular signaling pathways involved in the regulation of cell mechanics are likely initiated at the cell surface. Partial actin disassembly could be attributed to an electrically induced increase in $[Ca^{2+}]_i$. Changes in $[Ca^{2+}]_i$ can be mediated by a variety of well-characterized mechanisms. First, membrane depolarization can activate voltage-gated Ca^{2+} channels (VGCC). These electrically

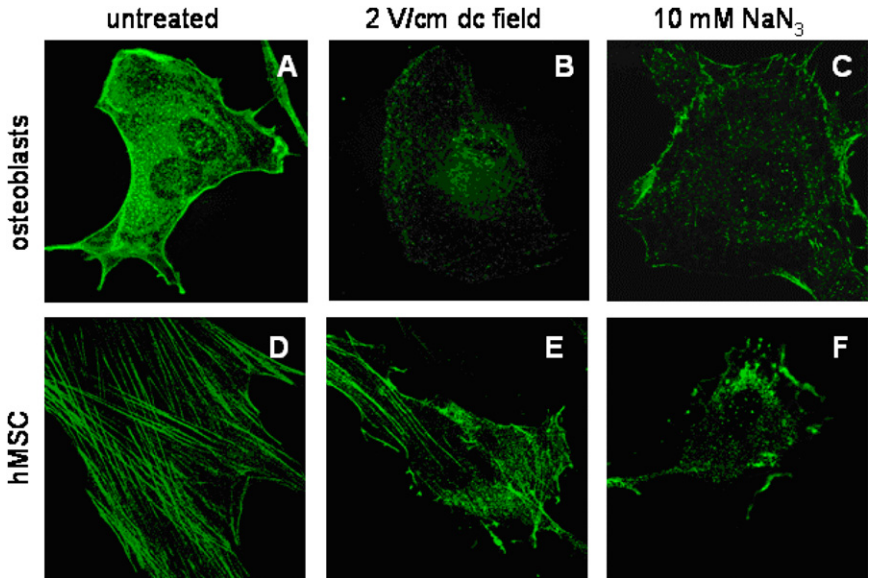

FIGURE 4 ERM protein redistribution in response to an electric field. Osteoblasts are shown in the upper row, and hMSCs in the lower row. Immunofluorescently labeled ezrin, radixin, and moesin proteins were uniformly distributed across the osteoblast membrane, likely due to high density ERM binding sites on the dense actin meshwork contiguous to the membrane (*A*). In contrast, in normal hMSCs ERM linkers were found localized only along the stress fibers adjacent to the juxtaposed membrane (*D*). After cell stimulation with a 2 V/cm field for 60 min, the amount of active (phosphorylated membrane-bound) ERM proteins seemed to decrease in osteoblast (*B*) as well as in hMSC (*E*). Similar effect was achieved by ATP depletion using 10 mM sodium azide and 10 mM 2-deoxyglucose in osteoblasts (*C*) and hMSCs (*F*). All images are 100 × 100 μm in size.

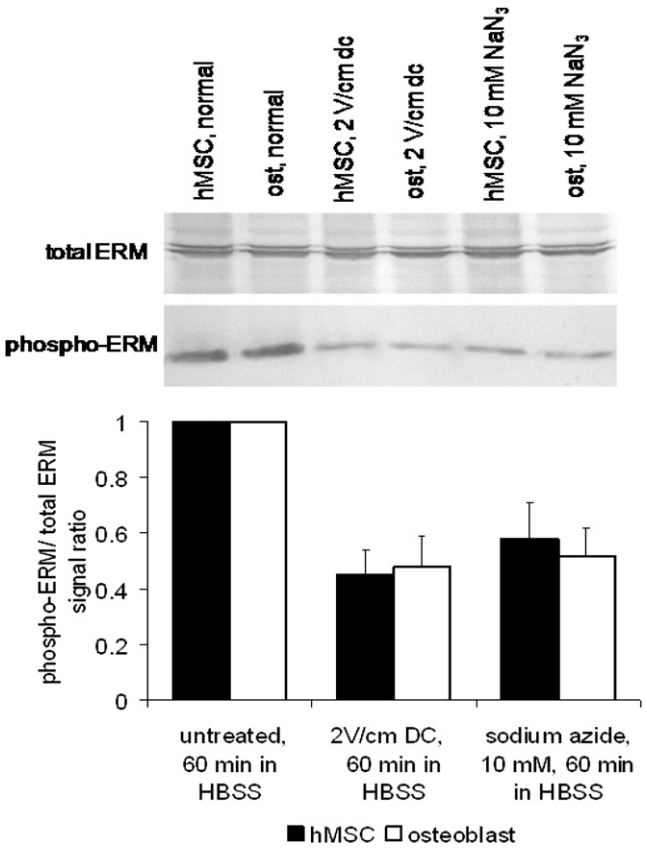

FIGURE 5 Electrically induced ERM protein inhibition. Immunoblotting of total and phosphorylated ERM proteins in osteoblasts and hMSC. Phosphorylation of inactive ezrin, radixin, and moesin in the cell cytoplasm allows their binding to both actin and transmembrane proteins, and dephosphorylation inhibits the membrane-cytoskeleton linker function. After cell exposure to a 2 V/cm dc electric field in HBSS or metabolic inhibitors sodium azide and 2-deoxyglucose for 60 min, cell lysates were prepared, and equal amounts of proteins per well were separated by SDS-PAGE, and the total and phosphorylated ERM proteins were detected by Western blotting (*top*) and quantified by densitometry scanning. The data for phospho-ERM immunoblot signal relative to untreated cell control and then normalized to the total ERM signal is shown as mean ± SE from four independent experiments (*bottom*). All treatments were significantly different from their respective controls ($p < 0.05$).

operated channels are excellent candidates for mediating the Ca^{2+} influx across the cell membrane induced by dc electric field (55). However, a 2 V/cm dc electric field is unlikely to directly activate voltage gated Ca^{2+} channels. For example, an osteoblasts ~50 μm in diameter exposed to a 2 V/cm dc field would experience ~5 mV change in the membrane potential, which is insufficient to cause VGCC activation. Second, an increase in $[Ca^{2+}]_i$ can be triggered by electrically induced activation of plasma membrane receptors that are coupled to phospholipase C (PLC). Activation of the PLC signaling cascade by an endogenous electric field results in release of Ca^{2+} from the endoplasmic reticulum, as shown earlier for osteoblasts (12). Third, Ca^{2+} influx can be mediated by stretch-activated cation channels, which can respond to electrically mediated cell morphological changes by the influx of cations including Ca^{2+}, as has been shown for several cell types (11,12). Therefore, both Ca^{2+} influx and Ca^{2+} release from intracellular storage can both contribute to increases in $[Ca^{2+}]_i$ in response to an electrical stimulation.

The details of actin dynamics depend on the original actin cytoskeleton structure. For example, stiff actin stress fibers in hMSCs seem to be relatively more susceptible to an external electrical field than a softer but more stable actin meshwork found in osteoblasts. As a result, the cell elasticity decreases more rapidly in stem cells by ~70% as compared to only a ~30% decrease in osteoblasts during the same 30 min electric field exposure. This could occur because different actin-binding proteins expressed in these cells and responsible for distinct F-actin organization patterns can have different sensitivity to the $[Ca^{2+}]_i$ (56,57). In addition, the magnitude and dynamics of the $[Ca^{2+}]_i$ elevation itself in response to an electrical stimulation can be very different in these cell types. For example, robust $[Ca^{2+}]_i$ oscillations are evident in hMSCs but not in osteoblasts (18).

The effect of electrical stimulation on actin cytoskeleton becomes more complicated in the presence of serum. Unlike simple electrically induced actin disassembly in the serum-free condition, redistribution of polymeric actins takes place when the cell is exposed to a dc field in the medium with 15% fetal bovine serum. We observed polymeric actin accumulation at the cathode side of the cell with concomitant actin depolymerization at the anode side. This actin redistribution might indicate directional serum-dependent cell electromigration toward the cathode, which has been reported elsewhere (15). Many cell membrane receptors have been reported to be redistributed in response to a dc electric field (10), and many growth factors (e.g., EGF, FGF, TGF-β1) may bind to appropriate receptors to trigger signaling pathways and to produce local changes in actin dynamics. The resulting cell

TABLE 1 Morphological parameters alteration of electrically stimulated and drug treated cells in HBSS

	hMSC		Osteoblast	
	Area $\times 10^3$ μm^2	Form factor	Area $\times 10^3$ μm^2	Form factor
Untreated cell	6.8 ± 1.8	0.25 ± 0.06	1.5 ± 0.7	0.42 ± 0.07
2 V/cm dc field (40 min)	6.4 ± 1.6	0.19 ± 0.06	1.3 ± 0.6	0.17 ± 0.06*
Ionomycin (10 μM)	3.9 ± 1.4*	0.14 ± 0.04*	0.7 ± 0.5*	0.06 ± 0.02*
Sodium azide (10 mM)	5.9 ± 1.8	0.27 ± 0.07	1.6 ± 0.9	0.06 ± 0.03*

Values represent mean ± SE from 14–19 cells to determine the form factor, and 75–90 cells to measure the area for each condition.
*Significantly different from respective normal (untreated) cells ($p < 0.05$).

galvanotaxis thus requires serum-derived growth factors, and involves asymmetric actin polymerization/depolymerization (15). We report an average decrease in the cell elasticity, focusing on only one of several physiologically relevant mechanisms of electrically mediated effects on actins. Although we did not characterize quantitatively cell migration in this study, we found that stem cells show less actin redistribution (and therefore migration) activity than osteoblasts under the similar experiment condition. This may be explained by a stronger hMSC adhesion to the substrate compared to osteoblasts as evidenced by a higher number and size of focal adhesions in hMSC (see Fig. 2 *B*). We also found no discernible effects of electric field on either intermediate filaments or microtubule structure. Unlike actins, these cytoskeleton components have been shown to have only a minor contribution to the cellular elasticity (41,48).

Electric field seems to affect the mechanical characteristics of another important cell component – the plasma membrane, which plays a crucial role in cell homeostasis: endo- and exocytosis, signaling, cell adhesion, and motility. The membrane mechanical performance in all these functions is coordinated by its interaction with cell cytoskeleton. Membrane is physically attached to actin cytoskeleton at focal adhesion sites as well as by specific linker proteins such as spectrin, ERM proteins, and myosin-I. The most likely candidates for the membrane-cytoskeleton coupling in eukaryotic cells are the ERM family proteins abundantly present in the cell cytoplasm. On phosphorylation these small (~80 kDa) molecules can bind both to polymeric actins and integral transmembrane proteins. Inhibition of the linker proteins by energy depletion may result in membrane separation from the cytoskeleton and subsequent cell membrane blebbing (58). Two cell types used in our study differ considerably in the membrane-cytoskeleton interaction. Thick actin stress fibers in stem cells provide a significant strength to the cytoskeleton, but relatively few binding sites for the ERM linkers. In contrast, a closely packed actin network in osteoblasts provides a high density binding sites for the ERM proteins, as immunofluorescently visualized (see Fig. 4). Osteoblasts exhibit an overall stronger mechanical coupling between the membrane and cytoskeleton than hMSCs, as proved by the tether extraction experiments. Indeed, when cells are subjected to energy deprivation, and the ERM linkers are dephosphorylated and inhibited, we observe an increase in the tether length in osteoblasts, suggesting membrane separation from the cytoskeleton. In contrast, in hMSCs this treatment does not cause any further increase in the membrane tether length primarily due to the originally very weak membrane-cytoskeleton interaction in this cell type. Similar effects on the membrane mechanics are produced by application of an electric field, which seems to induce an ATP depletion and leads to dephosphorylation and inhibition of the ERM linker proteins. Western blotting experiments confirm a reduced level of the ERM protein phosphorylation in both cell types after either an electrical stimulation or a biochemical ATP depletion. Thus, an electrical stimulation results in a decrease in the intracellular ATP level, inhibition of ERM proteins, and membrane separation from the cytoskeleton – this effect is especially noticeable in osteoblasts. Clearly, disruption of actin cytoskeleton itself also results in the membrane dissociation from the cytoskeleton (41). However, we measured a statistically significant tether length increase in osteoblasts after just 30 min of an electric field exposure when only a minimal actin rearrangement is observed. At a longer field exposure, both actin disassembly and ERM unbinding contribute to the membrane separation from the cytoskeleton.

The exact mechanism of ATP depletion in response to an electric stimulation is not clear. At least two potential mechanisms could be postulated. First, a decrease in the intracellular ATP may be due to transiently intensive ATP consumption by the cellular biomolecular machinery (e.g., transmembrane ion pumps) in response to dc field-mediated changes in the cell metabolism. Second, electrically induced ATP release from cells has been established and reported (47,50). ATP can be released through exocytosis mechanisms (e.g., secretory vesicles), specific ATP-transporting systems such as anion channels, or even transient electrophoretic membrane damage (59,60). Interestingly, the electric field-induced ATP release can have some paracrine and autocrine effects on the cells such as activation of purinergic receptors leading to a transient $[Ca^{2+}]_i$ elevation. For example, autocrine ATP signaling has been shown to play an important role for Ca^{2+} homeostasis in hMSC (61). In addition, multiple feedback loops in the electric field-induced cell biomechanical changes are likely. Both ATP-dependent P2X ligand-gated channels (50) and morphologically sensitive stretch-activated cation channels can contribute to an Ca^{2+} influx into the cell during an electrical stimulation. In turn, the influx of Ca^{2+} may interfere with glycolysis in the cytoplasm and aerobic respiration in mitochondria (62). The Ca^{2+}-mediated actin depolymerization further enhances the ATP depletion-driven membrane separation from the cytoskeleton. Details of the specific mechanisms responsible for modulated of the cell biomechanics by an electric field remain to be elucidated. Overall, the effect of an electric field on the cellular mechanical properties is a result of intricate interplay of events involving at least two major molecular mediators—Ca^{2+} and ATP. Therefore, changes in the membrane and the cytoskeleton mechanics are concurrent during cell exposure to an electric field.

Generally, the effect of an electrical stimulation can be regulated by changing the field strength. Outcome of cell exposure to dc fields of strengths in the range 1–3 V/cm is qualitatively analogous. A lower field strength requires more time to achieve a similar modulation of the cellular mechanical properties. The proposed model of dc field effects on the cellular mechanics is presented schematically in Fig. 6. It attempts to incorporate the already established electrical effects such as cell surface receptor redistribution,

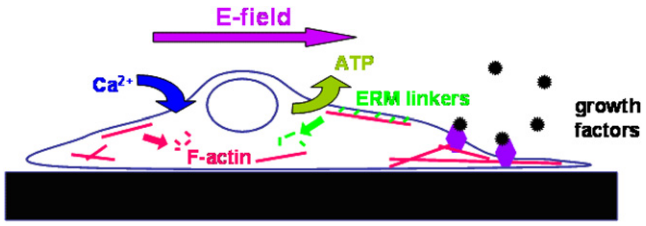

FIGURE 6 Schematic for electrocoupling mechanisms of cell mechanics modulation by electric field. External electric field induces an increase in the cytosolic calcium concentration mediated either by Ca^{2+} influx through plasma membrane or Ca^{2+} release from intracellular store. An elevated intracellular Ca^{2+} level depolymerizes the F-actins and decrease the cell elasticity. If present (e.g., cell electrical exposure with serum), growth factors could bind to electrically redistributed plasma membrane receptors and trigger a local increase in actin polymerization. Redistribution of the membrane receptors and actins in response to an electric field may mediate serum-dependent cell electromigration. In addition, an electrical stimulation causes intracellular ATP depletion, for example, by ATP release, which in turn leads to inhibition of the ERM linkers' binding properties and their dissociation from the membrane and actin cytoskeleton. Resultant membrane separation from the cytoskeleton and effectively decreased membrane tension are attributed both to electrically induced downregulation of active ERM proteins and actin depolymerization. The exact details of these mechanisms may vary in different cell types.

actin cytoskeleton disassembly mediated by intracellular Ca^{2+} elevation, and what to our knowledge are new findings from this study that the membrane-cytoskeleton separation is caused by inhibition of the ERM linkers through intracellular ATP depletion. The exact details of this mechanism may vary in different cell types (e.g., degree and rate of actin reorganization, original membrane-cytoskeleton adhesion strength, Ca^{2+} signaling pathways), and also biochemical environment (e.g., with or without serum).

One important conclusion of this study is that the effect of an electrical stimulation is cell type-dependent and reversible. This observation may be used to explain the synergistic osteogenic hMSC differentiation by application of a low intensity electrical stimulation (18). For example, as the stress fibers seem less stable than thin microfilaments, they may be disassembled first under an electrical exposure. This could bring the cell elastic and structural properties closer to those of fully differentiated osteoblasts. Electrically induced membrane dissociation from the cytoskeleton and subsequently a decrease in the membrane tension can then enhance endocytosis and transmembrane trafficking of soluble osteogenic factors. Cell recovery in the osteogenic medium after each a short-term electrical exposure will result in a further rearrangement of actins and ERM proteins into the osteogenic-type pattern. In contrast, neuronal-like cells exhibit weak actin cytoskeleton and relatively loose plasma membrane, as indicated by tether extraction experiments (63). Therefore, a higher strength electrical stimulation might be required to facilitate neurogenic differentiation of hMSC, which will maximally disrupt actin cytoskeleton and inhibit the ERM linkers. Thus, the electrical parameters of an electric field may be precisely controlled for selective manipulation of the mechanical properties of particular and preselected cell phenotype.

Finally, in addition to potentially facilitating stem cell differentiation into a particular lineage based on the modulated biomechanics, an electrical stimulation may also be useful for cell integration into environment with defined mechanical properties, including control of cell distribution patterns induced by directional electromigration. Such a physical control of cell behaviors may have important implications for tissue engineering by manipulating cell differentiation, mobility, and cell incorporation into engineered bioscaffolds, and eventual maturation of tissue substitute. An in-depth understanding of electrocoupling mechanisms that allows regulation of the cellular biophysical and biochemical properties will undoubtedly lead to a more effective development of electrotherapeutic techniques for regenerative medicine.

This work was supported, in part, by National Institutes of Health grant EB006067 and by a grant from the Office of Navy Research (N00014-06-1-0100). The AFM used to measure the cellular mechanical properties was purchased with Defense University Research Instrument Program grant N00014-04-1-0805.

REFERENCES

1. Boscolo, P., M. Di Gioacchino, L. Di Giampaolo, A. Antonucci, and S. Di Luzio. 2007. Combined effects of electromagnetic fields on immune and nervous responses. *Int. J. Immunopathol. Pharmacol.* 20:59–63.
2. Mycielska, M. E., and M. B. Djamgoz. 2004. Cellular mechanisms of direct-current electric field effects: galvanotaxis and metastatic disease. *J. Cell Sci.* 117:1631–1639.
3. Song, B., M. Zhao, J. Forrester, and C. McCaig. 2004. Nerve regeneration and wound healing are stimulated and directed by an endogenous electrical field in vivo. *J. Cell Sci.* 117:4681–4690.
4. Hotary, K. B., and K. R. Robinson. 1994. Endogenous electrical currents and voltage gradients in Xenopus embryos and the consequences of their disruption. *Dev. Biol.* 166:789–800.
5. Revest, P. A., H. C. Jones, and N. J. Abbott. 1994. Transendothelial electrical potential across pial vessels in anesthetized rats: a study of ion permeability and transport at the blood-brain barrier. *Brain Res.* 652:76–82.
6. Nuccitelli, R. 2003. A role for endogenous electric fields in wound healing. *Curr. Top. Dev. Biol.* 58:1–26.
7. Cho, M. R., H. S. Thatte, R. C. Lee, and D. E. Golan. 1996. Reorganization of microfilament structure induced by ac electric fields. *FASEB J.* 10:1552–1558.
8. Li, X., and J. Kolega. 2002. Effects of direct current electric fields on cell migration and actin filament distribution in bovine vascular endothelial cells. *J. Vasc. Res.* 39:391–404.
9. Cho, M. R., H. S. Thatte, R. C. Lee, and D. E. Golan. 1994. Induced redistribution of cell surface receptors by alternating current electric fields. *FASEB J.* 8:771–776.
10. Zhao, M., A. Dick, J. V. Forrester, and C. D. McCaig. 1999. Electric field-directed cell motility involves up-regulated expression and asymmetric redistribution of the epidermal growth factor receptors and is enhanced by fibronectin and laminin. *Mol. Biol. Cell.* 10:1259–1276.

11. Cho, M. R., H. S. Thatte, M. T. Silvia, and D. E. Golan. 1999. Transmembrane calcium influx induced by ac electric fields. *FASEB J.* 13:677–683.
12. Khatib, L., D. E. Golan, and M. Cho. 2004. Physiologic electrical stimulation provokes intracellular calcium increase mediated by phospholipase C activation in human osteoblasts. *FASEB J.* 18:1903–1905.
13. Titushkin, I. A., V. S. Rao, and M. R. Cho. 2004. Mode- and cell-type dependent calcium responses induced by electrical stimulus. *IEEE Trans. Plasma Sci. IEEE Nucl. Plasma Sci. Soc.* 32:1614–1619.
14. Sun, S., I. Titushkin, and M. Cho. 2006. Regulation of mesenchymal stem cell adhesion and orientation in 3D collagen scaffold by electrical stimulus. *Bioelectrochemistry.* 69:133–141.
15. Wang, E., M. Zhao, J. V. Forrester, and C. D. McCaig. 2003. Bi-directional migration of lens epithelial cells in a physiological electrical field. *Exp. Eye Res.* 76:29–37.
16. McCaig, C. D., L. Sangster, and R. Stewart. 2000. Neurotrophins enhance electric field-directed growth cone guidance and directed nerve branching. *Dev. Dyn.* 217:299–308.
17. Sauer, H., G. Rahimi, J. Hescheler, and M. Wartenberg. 1999. Effects of electrical fields on cardiomyocyte differentiation of embryonic stem cells. *J. Cell. Biochem.* 75:710–723.
18. Sun, S., Y. Liu, S. Lipsky, and M. Cho. 2007. Physical manipulation of calcium oscillations facilitates osteodifferentiation of human mesenchymal stem cells. *FASEB J.* 21:1472–1480.
19. Bai, H., C. D. McCaig, J. V. Forrester, and M. Zhao. 2004. DC electric fields induce distinct preangiogenic responses in microvascular and macrovascular cells. *Arterioscler. Thromb. Vasc. Biol.* 24: 1234–1239.
20. Zhao, M., H. Bai, E. Wang, J. V. Forrester, and C. D. McCaig. 2004. Electrical stimulation directly induces pre-angiogenic responses in vascular endothelial cells by signaling through VEGF receptors. *J. Cell Sci.* 117:397–405.
21. Ciombor, D. M., and R. K. Aaron. 2005. The role of electrical stimulation in bone repair. *Foot Ankle Clin.* 10:579–593.
22. Gordon, G. A. 2007. Designed electromagnetic pulsed therapy: clinical applications. *J. Cell. Physiol.* 212:579–582.
23. Janigro, D., C. Perju, V. Fazio, K. Hallene, G. Dini, et al. 2006. Alternating current electrical stimulation enhanced chemotherapy: a novel strategy to bypass multidrug resistance in tumor cells. *BMC Cancer.* 6::72.
24. Markov, M. S. 2007. Expanding use of pulsed electromagnetic field therapies. *Electromagn. Biol. Med.* 26:257–274.
25. Sisken, B. F., J. Walker, and M. Orgel. 1993. Prospects on clinical applications of electrical stimulation for nerve regeneration. *J. Cell. Biochem.* 51:404–409.
26. Lee, R. C., D. J. Canaday, and H. Doong. 1993. A review of the biophysical basis for the clinical application of electric fields in soft-tissue repair. *J. Burn Care Rehabil.* 14:319–335.
27. McCaig, C. D., A. M. Rajnicek, B. Song, and M. Zhao. 2005. Controlling cell behavior electrically: current views and future potential. *Physiol. Rev.* 85:943–978.
28. Huang, H., R. D. Kamm, and R. T. Lee. 2004. Cell mechanics and mechanotransduction: pathways, probes, and physiology. *Am. J. Physiol. Cell Physiol.* 287:C1–C11.
29. Janmey, P. A., and C. A. McCulloch. 2007. Cell mechanics: integrating cell responses to mechanical stimuli. *Annu. Rev. Biomed. Eng.* 9:1–34.
30. Lim, C. T., E. H. Zhou, and S. T. Quek. 2006. Mechanical models for living cells—a review. *J. Biomech.* 39:195–216.
31. Ingber, D. E. 2006. Cellular mechanotransduction: putting all the pieces together again. *FASEB J.* 20:811–827.
32. Orr, A. W., B. P. Helmke, B. R. Blackman, and M. A. Schwartz. 2006. Mechanisms of mechanotransduction. *Dev. Cell.* 10:11–20.
33. Wang, J. H., B. P. Thampatty, J. S. Lin, and H. J. Im. 2007. Mechanoregulation of gene expression in fibroblasts. *Gene.* 391:1–15.
34. Jena, B. P. 2007. Secretion machinery at the cell plasma membrane. *Curr. Opin. Struct. Biol.* 17:437–443.
35. Morris, C. E., and U. Homann. 2001. Cell surface area regulation and membrane tension. *J. Membr. Biol.* 179:79–102.
36. Raucher, D., and M. P. Sheetz. 1999. Characteristics of a -membrane reservoir buffering membrane tension. *Biophys. J.* 77: 1992–2002.
37. Sun, M., N. Northup, F. Marga, T. Huber, F. J. Byfield, et al. 2007. The effect of cellular cholesterol on membrane-cytoskeleton adhesion. *J. Cell Sci.* 120:2223–2231.
38. Sheetz, M. P., J. E. Sable, and H. G. Döbereiner. 2006. Continuous membrane-cytoskeleton adhesion requires continuous accommodation to lipid and cytoskeleton dynamics. *Annu. Rev. Biophys. Biomol. Struct.* 35:417–434.
39. Titushkin, I., and M. Cho. 2006. Distinct membrane mechanical properties of human mesenchymal stem cells determined using laser optical tweezers. *Biophys. J.* 90:2582–2591.
40. Shieh, A. C., and K. A. Athanasiou. 2003. Principles of cell mechanics for cartilage tissue engineering. *Ann. Biomed. Eng.* 31:1–11.
41. Titushkin, I., and M. Cho. 2007. Modulation of cellular mechanics during osteogenic differentiation of human mesenchymal stem cells. *Biophys. J.* 93:3693–3702.
42. Hutter, J. L., and J. Bechhoefer. 1993. Calibration of atomic-force microscope tips. *Rev. Sci. Instrum.* 64:1868–1873.
43. Reference deleted in proof.
44. Radmacher, M. 2002. Measuring the elastic properties of living cells by the atomic force microscope. *Methods Cell Biol.* 68:67–90.
45. Neuman, K. C., and S. M. Block. 2004. Optical trapping. *Rev. Sci. Instrum.* 75:2787–2809.
46. Coates, T. D., R. G. Watts, R. Hartman, and T. H. Howard. 1992. Relationship of F-actin distribution to development of polar shape in human polymorphonuclear neutrophils. *J. Cell Biol.* 117:765–774.
47. Sauer, H., R. Stanelle, J. Hescheler, and M. Wartenberg. 2002. The DC electrical-field-induced Ca(2+) response and growth stimulation of multicellular tumor spheroids are mediated by ATP release and purinergic receptor stimulation. *J. Cell Sci.* 115:3265–3273.
48. Trickey, W. R., T. P. Vail, and F. Guilak. 2004. The role of the cytoskeleton in the viscoelastic properties of human articular chondrocytes. *J. Orthop. Res.* 22:131–139.
49. Chen, H., I. Titushkin, M. Stroscio, and M. Cho. 2007. Altered membrane dynamics of quantum dot-conjugated integrins during osteogenic differentiation of human bone marrow derived progenitor cells. *Biophys. J.* 92:1399–1408.
50. Seegers, J. C., M. L. Lottering, A. M. Joubert, F. Joubert, A. Koorts, et al. 2002. A pulsed DC electric field affects P2-purinergic receptor functions by altering the ATP levels in in vitro and in vivo systems. *Med. Hypotheses.* 58:171–176.
51. Fiévet, B., D. Louvard, and M. Arpin. 2007. ERM proteins in epithelial cell organization and functions. *Biochim. Biophys. Acta.* 1773:653–660.
52. Louvet-Vallée, S. 2000. ERM proteins: from cellular architecture to cell signaling. *Biol. Cell.* 92:305–316.
53. Mangeat, P., C. Roy, and M. Martin. 1999. ERM proteins in cell adhesion and membrane dynamics. *Trends Cell Biol.* 9:187–192.
54. Poo, M. 1981. In situ electrophoresis of membrane components. *Annu. Rev. Biophys. Bioeng.* 10:245–276.
55. Cho, M. R. 2002. A review of electrocoupling mechanisms mediating facilitated wound healing. *IEEE Trans. Plasma Sci. IEEE Nucl. Plasma Sci. Soc.* 30:1504–1515.
56. dos Remedios, C. G., D. Chhabra, M. Kekic, I. V. Dedova, M. Tsubakihara, et al. 2003. Actin binding proteins: regulation of cytoskeletal microfilaments. *Physiol. Rev.* 83:433–473.
57. Paavilainen, V. O., E. Bertling, S. Falck, and P. Lappalainen. 2004. Regulation of cytoskeletal dynamics by actin-monomer-binding proteins. *Trends Cell Biol.* 14:386–394.

58. Chen, J., and M. C. Wagner. 2001. Altered membrane-cytoskeleton linkage and membrane blebbing in energy-depleted renal proximal tubular cells. *Am. J. Physiol. Renal Physiol.* 280:F619–F627.

59. Katsuragi, T., T. Tokunaga, M. Ohba, C. Sato, and T. Furukawa. 1993. Implication of ATP released from atrial, but not papillary, muscle segments of guinea pig by isoproterenol and forskolin. *Life Sci.* 53:961–967.

60. Wang, Y., R. Roman, S. D. Lidofsky, and J. G. Fitz. 1996. Autocrine signaling through ATP release represents a novel mechanism for cell volume regulation. *Proc. Natl. Acad. Sci. USA.* 93:12020–12025.

61. Kawano, S., K. Otsu, A. Kuruma, S. Shoji, E. Yanagida, et al. 2006. ATP autocrine/paracrine signaling induces calcium oscillations and NFAT activation in human mesenchymal stem cells. *Cell Calcium.* 39:313–324.

62. Wojtczak, L. 1996. The Crabtree effect: a new look at the old problem. *Acta Biochim. Pol.* 43:361–368.

63. Dai, J., M. P. Sheetz, X. Wan, and C. E. Morris. 1998. Membrane tension in swelling and shrinking molluscan neurons. *J. Neurosci.* 18:6681–6692.